AMERICAN SOCIETY FOR MICROBIOLOGY
Journals.ASM.org

Activation of Store-Operated Calcium Entry and Mitochondrial Respiration by Enterovirus 71 Is Essential for Viral Replication

Bang-Yan Hsu,[1] Ya-Hui Tsai,[2] Ta-Chou Weng,[1], Szu-Hao Kung[1]*

[1]Department of Biotechnology and Laboratory Science in Medicine, National Yang Ming Chiao Tung University, Taipei 112304, Taiwan.

[2]Department of Surgery, Far Eastern Memorial Hospital, Pan-Chiao, New Taipei, Taiwan.

*Address correspondence to Fourth Author: szkung@nycu.edu.tw

ABSTRACT

Enterovirus (EV) infections disrupt cellular calcium (Ca^{2+}) homeostasis. The EV protein 2B is localized to the endothelium reticulum (ER) and causes depletion of ER Ca^{2+} stores. This depletion coincides with a substantial increase in cytosolic Ca^{2+} levels driven by extracellular Ca^{2+} influx. However, the precise mechanism underlying this influx remains elusive. In the present study, we demonstrated that EV71 infections induce store-operated Ca^{2+} entry (SOCE) by activating the Ca^{2+} sensor stromal interaction molecule 1 (STIM1), which subsequently interacts with Orai1, a plasma membrane Ca^{2+} channel. This finding was supported by confocal imaging, which revealed that STIM1, typically localized in the ER, becomes active and colocalizes with Orai1 at the PM in EV71-infected cells. Pharmacological inhibition of the STIM1–Orai1 interaction and knockdown of either STIM1 or Orai1 significantly reduced virus-induced cytosolic Ca^{2+} levels and viral replication. Global transcriptome analysis revealed that differentially expressed genes are

primarily associated with the mitochondrial electron transport chain (ETC) upon SOCE activation, contributing to enhanced ATP generation and oxygen consumption. This increase in mitochondrial Ca^{2+} levels is correlated with the mid-stage of virus infection. Furthermore, we demonstrated that high levels of mitochondrial Ca^{2+} influx led to apoptotic cell death favoring viral release at the late stage of virus infection. Finally, SOCE-dependent EV replication was observed in a mouse intestinal organoid culture, a more physiologically relevant cell system. Our results provide valuable insights into the mechanism through which EV infections induce SOCE-mediated spatial and temporal control of Ca^{2+} signaling, substantially affecting the virus life cycle.

IMPORTANCE

Host cell cellular calcium (Ca^{2+}) signals play crucial roles in various steps of virus life cycles, including entry, replication, and exit. Enterovirus (EV) requires increased cytosolic Ca^{2+} levels for efficient replication, but the precise mechanisms underlying the association between Ca^{2+} levels and EV replication remain elusive. Using EV71 as a model virus, we demonstrated that EV71 infection elevated cytosolic Ca^{2+} levels through store-operated Ca^{2+} entry activation and progressive Ca^{2+} mobilization to mitochondria. This led to the upregulation of electron transport chain activity, which is essential for viral replication and apoptotic cell death, facilitating viral release during the mid- and late stages of the infectious cycle, respectively. These findings substantially enhance the understanding of how EVs co-opt host cell mechanisms to promote their own life cycle. STIM1 and Orai1 may be novel targets for broad-spectrum host-directed therapeutics against EVs and other viruses that employ similar replication mechanisms.

INTRODUCTION

Enteroviruses (EVs) are nonenveloped, positive-strand RNA viruses belonging to the genus *Enterovirus* of the family *Picornaviridae*. EVs consist of many human pathogens, including poliovirus, coxsackie A and B viruses, echoviruses, numbered EVs, and rhinoviruses[1]. Diverse EVs can cause a wide array of clinical manifestations ranging

from mild illnesses to more severe and even life-threatening diseases, such as myocardidits, meningitis, encephalitis and acute paralysis. Among EVs, EV71 (or EV-A71) infections have caused several outbreaks of hand, foot and mouth disease, with a notable proportion of infected infants and young children manifesting severe neurological complications and even consequent death, mainly in the Asia-Pacific region [1, 2]. However, currently there are no approved antiviral agents available against EV infections.

Intracellular calcium (Ca^{2+}) concentration plays a crucial role in regulating various cellular functions involved in physiological and pathological states. Viruses, as obligate intracellular parasites, have developed strategies to manipulate Ca^{2+} signaling and Ca^{2+}-dependent processes to promote their own life cycles [3, 4]. Enterovirus (EV) infections lead to considerable alterations in cellular Ca^{2+} homeostasis, including increased permeability of the endoplasmic reticulum (ER). This results in the depletion of Ca^{2+} stores in the ER, causing outflow of stored Ca^{2+} into cytoplasm and induction of a vast influx of extracellular Ca^{2+}. These changes contribute to increased cytosolic Ca^{2+} concentrations [5, 6, 7, 8, 9]. Disruption in Ca^{2+} homeostasis caused by EV infection is pivotal in viral replication. The use of Ca^{2+} chelators was reported to substantially reduce the production of viral proteins and progeny viruses [10]. Studies have demonstrated that EV 2B proteins play a pivotal role in increasing cytosolic Ca^{2+} levels. These proteins act as viroporins, a type of virus-encoded pore-forming protein [11, 12, 13]. EV 2B proteins are small, integral membrane polypeptides consisting of approximately 99 amino acids. They contain two hydrophobic regions connected by a short stem loop. One of these hydrophobic regions is likely to form an amphipathic alpha helix, whereas the other is likely to form a complete hydrophobic helix. This helix–loop–helix motif of 2B is believed to be responsible for its ability to form transmembrane pores through oligomerization [11]. In EV-infected cells, 2B proteins localize in membranes derived from the ER and Golgi apparatus. The pore-forming activity of 2B in these organelle membranes results in a decrease in Ca^{2+} stores in the ER and Golgi apparatus [11, 14], and is thus functionally associated with viral replication and release [8, 15, 14]. The single expression of EV 2B is sufficient to recapitulate the changes in Ca^{2+} homeostasis observed in EV-infected cells

[7, 8]. However, the molecular mechanism underlying the EV 2B–induced increase in cytosolic Ca^{2+} levels that supports viral replication and release remains elusive.

The coordinated regulation of Ca^{2+} release from the ER and subsequent entry of Ca^{2+} across the plasma membrane (PM) to replenish ER stores is referred to as store-operated calcium entry (SOCE). SOCE is a homeostatic cellular mechanism that helps maintain appropriate Ca^{2+} levels in the ER to facilitate Ca^{2+}-mediated signaling [16].Two protein families, stromal interaction molecules (STIMs) and Ca^{2+} release-activated Ca^{2+} modulators (Orais), are responsible for activating SOCE [16, 17]. STIM proteins act as sensors for Ca^{2+} levels in the ER. When Ca^{2+} is depleted in the ER [18], STIM proteins aggregate into multiple puncta that translocate close to the PM. Orai, an essential pore-forming component of SOCE, translocates to the same STIM-containing structures during Ca^{2+} depletion in the ER and mediates extracellular Ca^{2+} entry. To date, three isoforms of Orai (1–3) and two isoforms of STIM (1 and 2) have been identified in mammals.STIM1 levels are higher than STIM2 levels in most tissues. Moreover, STIM1 and Orai1 are sufficient for the generation of Ca^{2+}-release-activated Ca^{2+} currents, making Orai1 the primary channel activated by Ca^{2+} store release and STIM1 activation [19].

Given that EV 2B protein resides in the ER and that EV-infected or 2B-expressing cells experience an influx of extracellular Ca^{2+}, we investigated whether the ER–PM connection is involved in the increased cytosolic Ca^{2+} levels in the presence of EV 2B, i.e., SOCE activation, is involved in increased cytosolic Ca^{2+}. In the present study, we used EV71 known to cause disrupted Ca^{2+} homeostasis as a model [20, 21]. We demonstrated that EV-infected cells activate SOCE, with this activation mediated by the interaction between STIM1 and Orai1. To understand the downstream Ca^{2+} signaling events that support viral replication, we performed bulk RNA-sequencing (RNA-seq) to analyze the transcriptome of EV71-infected cells and the transcriptional reprograming of a specific SOCE inhibitor AnCoA4. We determined that SOCE activation led to an increase in mitochondrial Ca^{2+} levels, thereby promoting ATP production and cellular respiration by transcriptionally upregulating a panel of genes encoding mitochondrial electron transport chain (ETC) complexes at 6 h postinfection. Treatment with oligomycin, an inhibitor of ATP production, reduced viral replication in a dose-dependent manner, indicating that

increased ATP production is required for efficient EV71 replication. At 12 h postinfection, Ca^{2+} influx led to mitochondrial Ca^{2+} overload, resulting in the activation of intrinsic apoptosis that facilitated virus egress and pathogenesis. This SOCE- and mitochondria Ca^{2+}-dependent viral replication phenomenon was also noted in other EV serotypes. Finally, we observed SOCE-dependent upregulation of ETC complexes and EV replication in a mouse intestinal organoid model that mimicked the in vivo environment [22].

MATERIALS AND METHODS

Cells and Viruses

Rhabdomyosarcoma (RD) cells (ATCC,CCL-13) and HeLa cells (ATCC,CCL-2) were cultured as described elsewhere [23]. Human EV stocks used in this study included EV71 (strain BrCr), coxsackievirus A16 (CVA16), CVB3 and echovirus serotype 30 (Echo30) as reported previously [23]. A mouse-adapted EV71 MP4 strain [24] was provided from Dr. Jen-Ren Wang (National Cheng Kung University, Taiwan). All virus stocks were titrated on RD cells by 50% tissue culture infectious dose ($TCID_{50}$) assay.

Ca^{2+} fluorescence dyes assay

RD and HeLa cells were infected with EV71 at a specified multiplicity of infection (MOI) in 24-well plates for the indicated durations. Cells were incubated with the cytosolic Ca^{2+} dye Fluo-8 at 1 µM or the mitochondrial Ca^{2+} dye Rhod-2 AM at 3 µM, both for 30 min at at 37°C. The emitted fluorescence resulting from Fluo-8 or Rhod-2 AM staining was observed using a fluorescence microscope (DM6000B,Leica) with a 488-nm or 543-nm filter, respectively. The fluorescence intensity was quantified using MetaMorph software (Molecular Devices, Downington, PA).

Ectopic expressions of STIM1 and Orai1 for confocal analysis

Plasmid encoding enhanced green fluorescent protein (EGFP)-labeled STIM1 (pEGFP-STIM1) and monomeric red fluorescent protein (mOrange)-labeled Orai1 (pmOrange-Orai1) were provided by Dr. Meng-Ru Shen (National Cheng Kung University, Taiwan). The colocalzation of STIM1 and Orai1 was observed by confocal microscopy. See Text S1 for details.

RNA-seq

RNA extraction was performed using RNeasy Kits (Qiagen, Hamburg, Germany), and RNA-seq libraries were prepared using the Universal Plus mRNA Seq Preparation kit (Tecan). RNA-seq was performed using the NovaSeq 6000 platform (Illumina, San Diego, CA) in accordance with the manufacturer's protocol, with 2 × 150-bp paired-end sequencing. Reads were aligned to the GRCm38 build of the human genome by using CLC Genomics Workbench v10 (Qiagen).

Differential expression analysis

The expression level of each gene was examined by fragment length, determined by read counts, and normalized using the fragments per kilo base of transcript per million mapped fragments variation method. Genes with significant changes in mRNA levels were identified on the basis of a false discovery rate cutoff of 0.05 and a fold change of 2. Gene set enrichment analysis was conducted using the Database for Annotation, Visualization, and Integrated Discovery (DAVID, https://david.ncifcrf.gov/) [25]. Biological processes with corrected p-values of ≤ 0.05 were considered significantly enriched pathways.

Measurement of cellular respiration

Cellular respiration was measured using the Seahorse XF Cell Mito Stress Test Kit (Agilent, Santa Clara, CA) in accordance with the manufacturer's instructions. HeLa cells

seeded in XFe 24-well microplates were infected with EV71 stock at an MOI of 5 for 6 h. The microplates were placed in a non-CO_2 incubator at 37°C for 1 h prior to measurement. Cellular respiration was analyzed using sequential injections of 2 µM oligomycin (an ATP synthase blocker), 1 µM carbonyl cyanide-p-trifluoromethoxyphenylhydrazone (FCCP, an activator of the uncoupling of the inner mitochondrial membrane), and 0.5 µM rotenone/antimycin A (inhibitors of complexes I and III). The oxygen consumption rate (OCR) was determined by Seahorse XFe24 Extracellular Flux Analyzer (Agilent).

Cultivation, infection and imaging of crypt organoids

Mouse intestinal stem cells were isolated following a method documented [26] and it is reported in the Text S1. The preparation and culture of mouse intestinal organoid followed a protocol described previously with certain modifications [22]. Briefly, mouse crypt organoids were seeded in differentiation medium consisting of Advanced DMEM/F12 (Invitrogen) containing growth factors as previously reported [26]. Crypt organoids were mixed with Matrigel (BD Bioscience) and plated in 12-well plates. The medium was changed every 2 days for 10-14 days. Differentiated mouse intestinal organoids were sheared mechanically by pipetting to enable sufficient apical exposure to virus inoculums. The organoids were inoculated with 200 µL EV71 MP4 strain (4×10^8 $TCID_{50}$/mL) for 2 h at 37°C. After the incubation, the organoids were washed with PBS and organoids were embedded in Matrigel with the differentiation medium at 37 °C for 48 h. The images were acquired by confocal microsopy (LSM880, Zeiss). See Text S1 for details.

Result

EV71 increases cytosolic Ca^{2+} levels through 2B protein

Previous studies have demonstrated that infection with poliovirus or coxsackievirus B increases cytosolic Ca^{2+} levels [5, 6]. In the current study, we used EV71 as a model virus. Our results revealed that the cytosolic Ca^{2+} levels significantly increased starting at 6 h

181 postinfection (p.i.) and continued to rise throughout the infection for 12 h, as indicated by
182 staining with the fluorescent Ca^{2+}-binding dye Fluo-8 (Fig. 1A, S1). To further identify the
183 source of Ca^{2+}, we added intracellular and extracellular Ca^{2+} chelating agents,
184 BAPTA-AM (referred to BAPTA hereafter) and EGTA, respectively, to the viral cultures.
185 Both treatments resulted in a marked reduction in cytosolic Ca^{2+} levels between 6 and 12
186 h p.i (Fig. 1A, S1), indicating that at least part of the increased cytosolic Ca^{2+} originated
187 from outside the infected cells. Viral 2B protein from several members of EVs causes
188 depleted Ca^{2+} stores in the ER and Golgi apparatus, resulting in an increase in cytosolic
189 Ca^{2+}. Thus, we investigated the effect of EV71 2B expression alone in RD cells and
190 identified an increase in cytosolic Ca^{2+} levels (Fig. 1B). Treatment with either BAPTA or
191 EGTA also significantly reduced Ca^{2+} levels during viral 2B expression (Fig. 1B). Together,
192 these data indicate that extracellular Ca^{2+} influx contributed to the increase in cytosolic
193 Ca^{2+} observed during EV71 infection and that the single expression of EV71 2B
194 recapitulated the effect caused by viral infections.

195 Orai1 and STIM1 are essential for EV71 replication

196 Several Ca^{2+} channels or transporters on the PM mediate Ca^{2+} influx from outside the
197 cells [27]. Among them, only SOCEs are activated by the link between ER-resident STIM1
198 and PM-resident Orai1. EV 2B localizes in the ER and reduces ER Ca^{2+} levels by forming
199 transmembrane pores. Thus, we hypothesized that SOCE machinery contributes to Ca^{2+}
200 influx extracellularly through the PM, resulting in the observed increase in cytosolic Ca^{2+}
201 levels in the EV71-infected and 2B-expressing cells. To validate this hypothesis, we
202 generated HeLa cells ectopically coexpressing STIM1 and Orai1 labeled with EGFP and
203 mOrange, respectively (Text S1). Thapsigargin (TG) was used as a control as it is known
204 to induce ER Ca^{2+} store depletion and activate SOCE by blocking the sarco/ER Ca^{2+}
205 -ATPase pump. Whereas the mock-infected cells exhibited a minimal level of STIM1-Orai1
206 colocalization, the infected HeLa-Orai1-STIM1 cells exhibited increased colocalization of
207 STIM1 and Orai1 (4.6% to 25.2%), consistent with that of the TG-treated cells (Fig. 2).
208 Moreover, the colocalization of STIM1 and Orai1 caused by EV71 infection was
209 substantially inhibited by the treatment of AnCoA4, a specific blocker of STIM1–Orai1

210 binding [28]. Subsequently, to investigate the role of SOCE in EV71 infection, we used
211 lentivirus-mediated RNA interference to generate stable STIM1- and Orai1-knockdown
212 cells, and the efficient knockdown effects were validated (Fig. S2). Knockdown of either
213 STIM1 or Orai1 resulted in marked reductions in EV71-induced cytosolic Ca^{2+} at 6 h p.i.,
214 compared with that of the scramble control (Fig. 3A). Likewise, viral protein expressions
215 were greatly reduced in the STIM1- and Orai1-knockdown cells over the scramble
216 controls, at both 6 h p.i. (Fig. 3B) and 12 h p.i. (Fig. 3C). Next, we investigated the
217 treatment of AnCoA4 on Ca^{2+} flux and viral replication. We observed that levels of
218 cytosolic Ca^{2+} were significantly reduced between 6 and 12 h p.i. in the infected cells by
219 AnCoA4 treatment compared with the levels in the untreated counterparts (Fig. 3D); this
220 finding is consistent with that for the cells treated with Ca^{2+}-chelating agents (Fig. 1A).
221 Viral replication was substantially attenuated after treatment with AnCoA4 at 6 h and 12
222 h p.i. in a dose-dependent manner relative to that of the untreated controls (Fig. 3E).
223 Taken together, these data indicated that EV71 infection activated the STIM1-Orai1
224 machinery, resulting in increased cytosolic Ca^{2+}, which is essential for viral replication.

225 Transcriptional Changes in EV71 infection following with AnCoA4 treatment

226 We initially analyzed the well-known SOCE–NFAT axis to explore downstream Ca^{2+}
227 signaling [28, 29], and found that it is independent of EV71 replication (Fig. S3).
228 Subsequently, we investigated the global transcript alterations between mock-infected
229 cells and EV71-infected cells and between EV71-infected cells and EV71-infected cells
230 treated with AnCoA4. We performed RNA-seq to identify differentially expressed genes.
231 A total of 86 genes with a fold change of >2 were identified. Gene set enrichment analysis
232 revealed that enriched functional clusters were significantly altered in both groups. These
233 were primarily associated with the mitochondrial ETC (Table 1), which consists of four
234 complexes (CI through CIV) that couple reduction–oxidation reactions, creating an
235 electrochemical gradient that leads to the generation of ATP. The identified genes encode
236 mitochondrial NADH dehydrogenases (MT-NDs), cytochrome B (CYB), and cytochrome c
237 oxidase subunit I (COI), which belong to mitochondrial ETC CI, CIII, and CIV,
238 respectively (Table 1). We next validated the results through RT-qPCR, which revealed

239 similar alterations in ND4, ND6, CYB, and COI transcripts following EV71 infection in the
240 absence or presence of AnCoA4 treatment (Fig. 4A). Moreover, the expression of EV71 2B
241 alone significantly upregulated the levels of ND6, CYB and COI transcripts, as EV71
242 infection did (Fig. 4B). The function of the mitochondrial ETC begins with CI that
243 catalyzes electron transfer from NADH to ubiquinone, which was discovered to be
244 particularly enriched in the analysis (Table 1). We additionally investigated mitochondrial
245 CI activity upon EV71 infection with or without AnCoA4 treatment and observed a
246 marked elevation or reduction in CI activity, respectively (Fig. 4C). Given that ATP is the
247 end product of the ETC, we analyzed the effect of SOCE on ATP levels and that of ATP
248 blockade on viral replication. We determined that the ATP level was significantly
249 increased following EV71 infection and reduced after AnCoA4 treatment (Fig. 4D).
250 Moreover, viral RNA and protein levels decreased after treatment with oligomycin, an
251 inhibitor of mitochondrial ATP synthase (complex V) [30, 31], in a dose-dependent
252 manner (Fig. 4E, F), indicating that ATP production is essential for EV71 replication.
253 Together, these findings indicate that the RNA levels of several components of ETC
254 complexes and ETC activity were enhanced following EV71 infection at 6 h p.i. and that
255 SOCE activation played a pivotal role in the process.

256 **OCR measurement**

257 Given that the upregulation of transcripts in mitochondrial ETC complexes during
258 EV71 infection affects the function of mitochondria, we assessed several functional ETC
259 parameters (indicated in the Fig. 5A) by using a live-cell Seahorse assay [30, 31] in
260 mock-infected cells, infected cells, and infected cells treated with AnCoA4 (Fig. 5B, C).
261 Levels of OCR in EV71-infected cells were increased compared to mock-infected cells and
262 reduced following AnCoA4 treatment (Fig. 5B). Concurrently, the relative levels of basal
263 and maximal respiration were also increased in EV71-infected cells and reduced by
264 AnCoA4 treatment (Fig. 5C). A similar trend of ATP production as those of the OCR and
265 basal/maximal respiration was observed (Fig. 5C). Proton leak, spare respiratory capacity,
266 and nonmitochondrial oxygen consumption remained unchanged. These results indicate
267 that the upregulated transcripts encoding the components of ETC complexes in the

268 EV71-infected cells were functionally active, leading to increased respiration and
269 enhanced bioenergy production, with this effect likely mediated through SOCE activation.

270 EV71 induced mitochondrial Ca^{2+} influx through SOCE

271 EV infections cause a progressive increase in mitochondrial Ca^{2+} during infection. In
272 isolated mitochondrial systems, the addition of Ca^{2+} enhances the activities of complexes
273 I, III, and IV as well as ATP production by more than two-fold [32, 33]. Therefore, we
274 hypothesized that the upregulated levels of the complex components (Table 1 and Fig. 4A)
275 are associated with Ca^{2+} influx into mitochondria. EV71-infected cells were stained with
276 Rhod-2 AM (referred to Rhod-2 hereafter) fluorescent dye to analyze the mitochondrial
277 Ca^{2+} levels at 6 and 12 h p.i. Depletion of ER Ca^{2+} stores by TG treatment resulted in an
278 increased level of mitochondrial Ca^{2+} compared with that in the mock control (Fig. 6A).
279 The infected cells displayed progressive elevations in mitochondrial Ca^{2+} during infection
280 that were significantly decreased after treatment with ruthenium red (RR), a specific
281 inhibitor of the mitochondrial Ca^{2+} uniporter (MCU) [10, 20] that allows the passage of
282 Ca^{2+} from the cytosol into mitochondria (Fig. 6A). A similar reduction in mitochondrial
283 Ca^{2+} levels was observed following AnCoA4 addition, implying a correlation of
284 mitochondrial Ca^{2+} influx with SOCE activation. This notion was supported by the
285 finding that the expression of viral 2B alone increased mitochondrial Ca^{2+} levels, which
286 were significantly decreased following treatment with RR or AnCoA4 (Fig. 6B). Moreover,
287 viral protein levels were decreased after treatment with 10 or 20 μM RR in a dose- and
288 time-dependent manner (Fig. 6C). Moreover, RR treatment reduced the ATP level
289 promoted by EV71 infection (Fig. 6D), supporting the notion that elevated mitochondrial
290 Ca^{2+} levels are associated with ATP production at 6 h p.i. Next, we analyzed a panel of
291 representative EV serotypes, namely CVA16, CVB3, and Echo9, for the
292 SOCE–mitochondrial Ca^{2+} axis. In all of these serotypes, we observed that blocking SOCE
293 activation by using AnCoA4 reversed mitochondrial Ca^{2+} influx (Fig. 6E), and RR
294 treatment reduced viral protein levels in a dose-dependent manner (Fig. 6F). These
295 findings indicate that EV-induced SOCE activation facilitates viral replication through
296 mitochondrial Ca^{2+} influx and consequent ATP elevation at 6 h p.i.

297 **SOCE activation is correlated with cell apoptosis and virus release during the late**
298 **phase of EV71 infection**

299 EV infections induce mitochondrial Ca^{2+} overload during the late stage of the virus
300 life cycle, leading to cell death [8, 10, 20]. We investigated whether this Ca^{2+} influx results
301 in mitochondrial Ca^{2+} overload and investigated its impact on cell fate and virus
302 production during the late phase of infection at 12 h p.i. EV71 infection markedly reduced
303 cell viability. This reduction in cell viability was reversed by AnCoA4 in a dose-dependent
304 manner (Fig. 7A). Consistent with this finding, the cell viability progressively decreased
305 as the MOIs of the virus infections increased, and all of these reductions were markedly
306 rescued by AnCoA4 treatment (Fig. 7B). Because mitochondrial Ca^{2+} overload triggers
307 apoptotic cell death, we measured the caspase activities in the EV71-infected cells at 12 h
308 p.i. after AnCoA4 treatment. AnCoA4 markedly reversed the EV71-induced activities of
309 caspase -3 and -9 but not those of -8, indicating that the virus-induced activation of the
310 intrinsic apoptosis pathway is at least partly mediated by SOCE-mediated mitochondrial
311 Ca^{2+} overload. Because the release of EV from cells is mediated by apoptosis through the
312 lytic mode, we investigated whether SOCE activation and mitochondrial Ca^{2+} influx
313 affect virus production. AnCoA4 or RR was added to cultures during EV71 infection, and
314 the cells and their supernatants were harvested at 12 h p.i. to enable measurement of the
315 titers of intracellular (InV) and extracellular virus (ExV), respectively. The ExV titer/total
316 viral titer (E/T) ratio was determined to investigate the virus release efficiency. In all
317 cases, treatment with either AnCoA4 or RR reduced the titers of ExV and InV in a
318 does-dependent fashion (Fig 7D, F). Importantly, either compound treatment resulted in
319 does-dependent reduction in the E/T ratio (Fig. 7E, G), suggesting that blockade of the
320 SOCE or mitochondrial Ca^{2+} influx led to greater inhibitory effects on the viral release
321 than on the total virus production. Together, these findings indicate that SOCE activation
322 and subsequent mitochondrial Ca^{2+} overload play a pivotal role in the induction of
323 apoptotic processes and facilitate the egress of virus progeny.

Mouse intestinal organoids infected with EV71

Given that all studies above were conducted using permissive cell lines, that is, RD and HeLa cells, we investigated Ca^{2+} signal–dependent viral replication in a more physiologically relevant cell culture system. We established a mouse intestinal organoid culture derived from isolated intestinal stem cell–containing crypt fractions to evaluate intestinal pathophysiology [22, 26, 34]. Single intestinal stem cells can be cultured into three-dimensional enteroids comprising all major differentiated cell types that can be found in the native intestinal organoid (Fig. 8A). However, EV infections are restricted by species barriers; human cells are susceptible to such infections, whereas mouse cells are typically resistant to them [35]. On the other hand, a mouse-adapted EV71 MP4 strain was demonstrated to efficiently infect mouse cell cultures and a mouse model [24, 36]. Thus, we used a mouse-adapted EV71 MP4 strain to inoculate our mouse intestinal enteroid cultures in the absence or presence of AnCoA4. Immunofluorescence staining was conducted, and the levels of viral antigen were analyzed through confocal microscopy. The viral antigen signals were well discernible in the infected-cells and significantly reduced after AnCoA4 treatment (Fig. 8B, C). In addition, the relative levels of viral RNA and representative ETC ND6, CYB and COI RNAs were analyzed. A similar trend of alteration in the viral RNA was observed as those of the viral antigen (Fig. 8C, D). The mouse ETC RNA levels were substantially increased following EV71 infection relative to that of the mock-infected control; the levels significantly declined upon treatment with AnCoA4 (Fig. 8E).

Figures

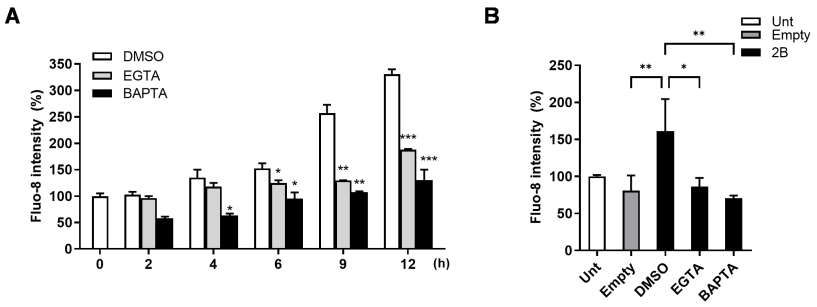

FIG 1 EV71 infection and viral 2B expression induced elevated cytosolic Ca^{2+} levels, which were reduced by treatment with Ca^{2+} chelators. (A) RD cells were infected with EV71 stock at an MOI of 2 for the indicated times in the presence of BAPTA (20 μM), EGTA (1 mM), or left untreated (DMSO treatment). (B) HeLa cells were transfected with the pFLAG-CMV-2 (empty) plasmid, pCMV-FLAG-2B (2B) plasmid, or left untransfected (Unt) for 40 h. For untransfected and empty controls, media were replaced with DMSO-containing media, and incubated for 8 h. For the pCMV-FLAG-2B -transfected cells, media were replaced with DMSO-, EGTA-, or BAPTA-containing medium, as indicated, and also incubated for 8 h. Cells were stained with the cytosolic Ca^{2+} fluorescent dye Fluo-8, and fluorescence was observed using a fluorescence microscope (Leica DM 600B) with intensities quantified relative to the mock-infected controls (A) or untransfected controls (B), both normalized by the number of cells stained with DAPI. Data represent mean values from experiments conducted in triplicate, with error bars indicating standard deviations (SDs). ***$p < 0.001$, **$p < 0.01$, *$p < 0.05$.

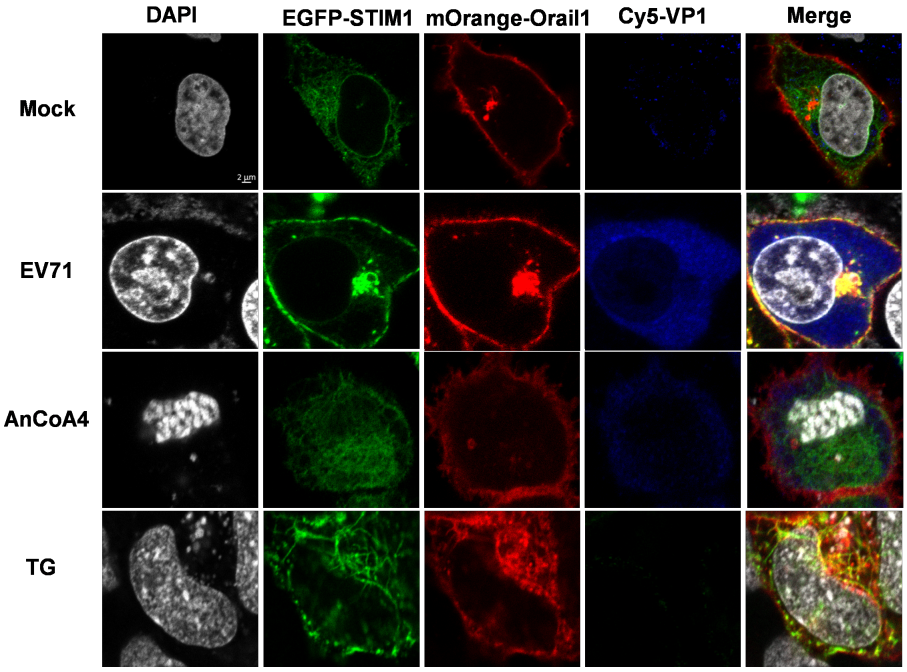

347

FIG 2 EV71 infection induced enhanced colocalization of STIM1 and Orai1. HeLa-STIM1-Orai1 cells coexpressing EGFP–STIM1 (green) and mOrange–Orai1 (red) were mock-infected or infected with EV71 at an MOI of 1 for 9 h in the absence or presence of AnCoA4 at 20 μM. Treatment with 5 μM TG for 15 min

served as a positive control for SOCE activation. Viral protein (blue) was detected using the anti-EV71 primary Ab followed by the Cy5-labeled secondary antibody. Colocalization of EGFP–STIM1 and mOrange-Orai1 is presented in yellow. Cell nuclei were stained with DPAI (white). Images were acquired using a Zeiss LSM880 confocal microscope. Bar, 2 μm.

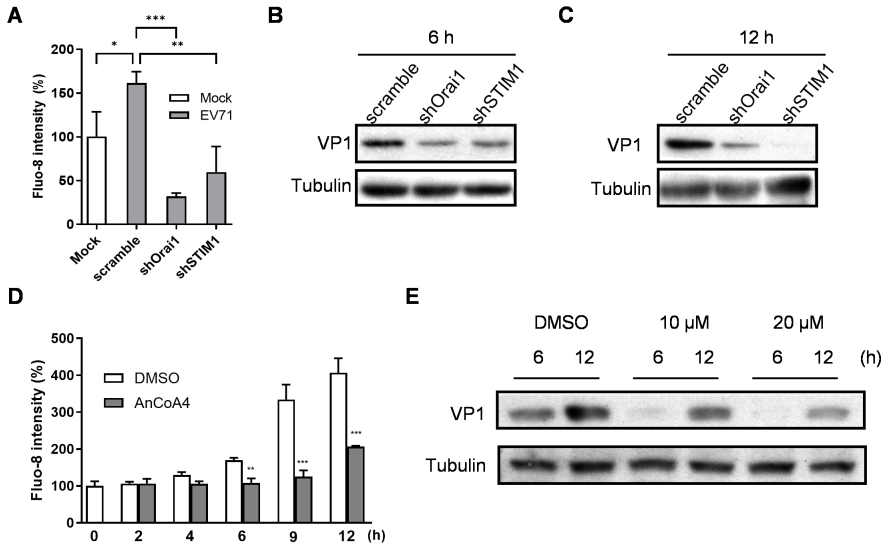

348

FIG 3 Both STIM1 and Orai1 were essential for EV71 replication. HeLa cells were transduced with lentivirus–shScramble, –shOrai1 or –shSTIM1 48 h prior to infection with EV71 at 0.5 MOI for 6 h (A, B) or 12 h (C). RD cells were infected with EV71 at 0.5 MOI for the indicated times, and left compound-free (DMSO treatment) or incubated with 20 μM AnCoA4 during the infection periods (D). RD cells were infected with EV71 at an MOI of 0.5 for 6 h and 12 h, and left compound-free (DMSO treatment) or treated with 10 or 20 μM AnCoA4 during the infection periods. Cells were stained with Fluo-8 for cytosolic Ca^{2+} measurement in (A, D), and relative fluorescence was quantified using the method described in the legend of Fig. 1. The experiments were conducted in triplicate, and shown as means ± SDs. ***$p < 0.001$,**$p < 0.01$, *$p < 0.05$. Cell lysates were harvested from each condition in (B, C, and E), and levels of viral VP1 protein and tubulin (the internal control) were measured by immunoblot analysis.

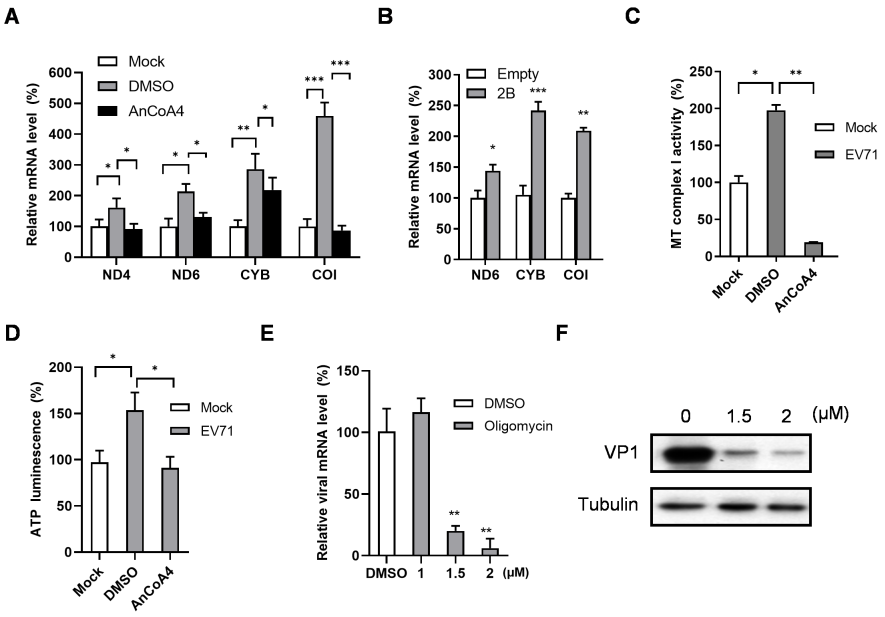

349

FIG 4 EV71 induced transcriptional and functional upregulation of mitochondrial ETC genes through SOCE machinery. (A) RD cells were infected with EV71 at an MOI of 0.5 for 6 h or mock infected. The infected cells were treated with 20 μm AnCoA4 or left untreated. (B) HeLa cells were transfected with empty or 2B-expressing plasmids for 48 h. Relative RNA levels of representative components of ETC complexes, as indicated, were determined through RT-qPCR by using total RNA prepared under each condition in (A, B) and shown as levels relative to those of mock-infected controls (A) or empty plasmid-transfected controls (B). HeLa cells were infected with EV71 at an MOI of 5 for 6 h and left untreated (DMSO treatment) or treated with 20 μM AnCoA4 or left untreated (DMSO treatment) (C, D). Mitochondria were isolated for the complex I activity assay and shown as levels relative to those of mock-infected controls (C). Cellular ATP activity was measured and reported as levels relative to those of mock-infected controls (D). HeLa cells were infected with EV71 at an MOI of 0.5 with oligomycin treated at the indicated concentrations or left untreated (DMSO treatment). Total RNA and cell lysates were collected at 6 h p.i. for RT-qPCR (E) and immunoblots (F), respectively. ***$p < 0.001$,**$p < 0.01$, *$p < 0.05$.

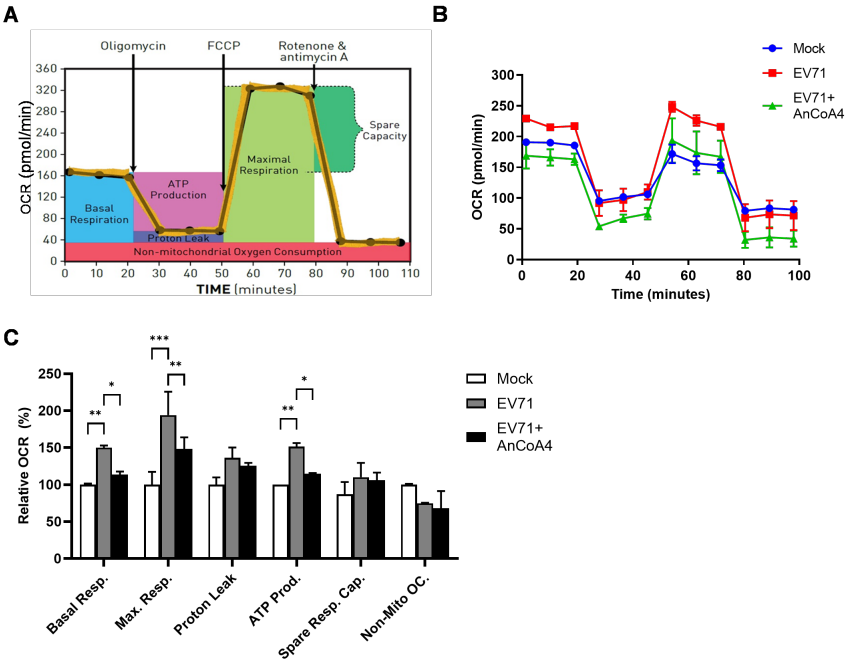

350

FIG 5 EV71-infected cells displayed increased mitochondrial respiration through the SOCE machinery. (A) Diagram illustrating the oxygen consumption rate (OCR) measured for the parameters including basal respiration, maximal respiration, proton leak, ATP production, spare respiratory capacity, and nonmitochondrial oxygen consumption of ETC function, by using the XFe24 Seahorse analyzer; this diagram was reproduced with permission. (B) HeLa cells were mock-infected or infected with EV71 (MOI = 5) for 6 h in the absence or presence of AnCoA4 at 20 μM. Oligomycin, FCCP, and antimycin A + rotenone were injected at the times indicated in (A). (C) The six parameters were analyzed following the manufacturer's instructions and are presented as percentages relative to the mock-infected cells. Data are presented as means ± SDs.

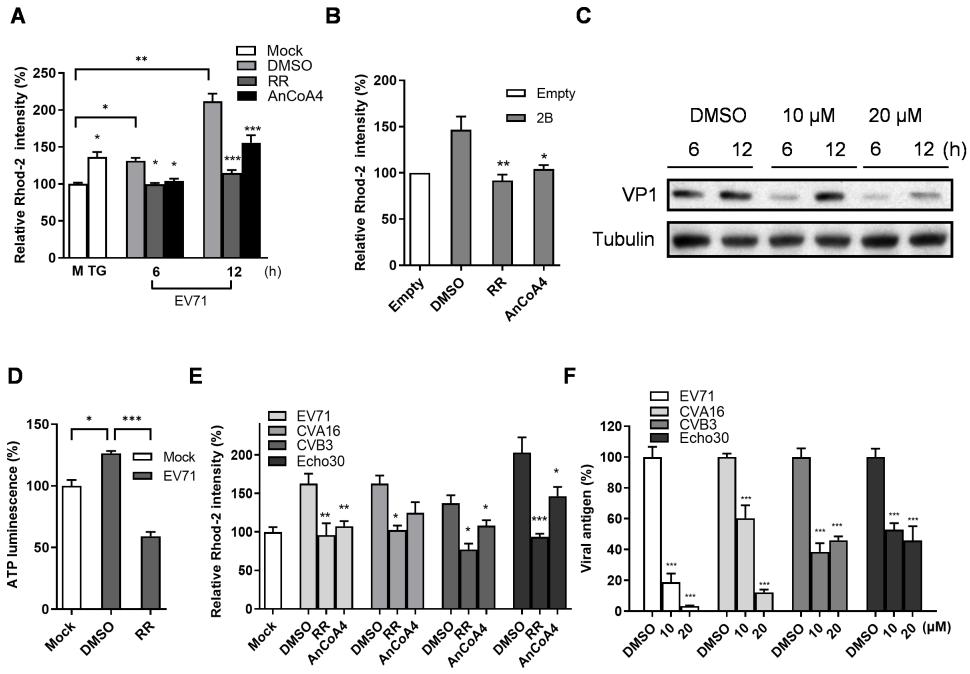

351

FIG 6 EV71 infections increased the mitochondrial Ca^{2+} influx that contributed to viral replication and ATP production at the mid-stage of the virus life cycle. (A) HeLa cells were treated with 10 μM RR, 20 μM AnCoA4, or left untreated (DMSO) during EV71 infection at an MOI of 0.5 for 6 h and 12 h and were then stained with Rhod-2. TG served as a positive control for Rhod-2 stain. The relative Rhod-2 fluorescence intensity of each condition was quantified relative to that of a mock-infected control (M), and normalized by the number of cells stained with DAPI. (B) HeLa cells were transfected with an empty or 2B-expressing plasmid for 40 h. The media were replaced with DMSO, 10 μM RR, or 20 μM AnCoA4-containing media for 8 h and then stained with Rhod-2. (C) RD cells were infected with EV71 at an MOI of 0.5 and treated with 10 or 20 μM RR or left untreated (DMSO). Cell lysates were collected at 6 and 12 h p.i., and levels of viral VP1 protein and tubulin (the internal control) were measured by immunoblot analysis. (D) HeLa cells were infected with EV71 at an MOI of 5 for 6 h and treated with 10 μM RR or left untreated. Cellular ATP activity was measured and reported as levels relative to those of the mock-infected control. (E, F) HeLa cells were infected with EV71, CVA16, CVB3, or Echo 30, each at an MOI of 1 for 6 h, and were treated with 10 μM RR, 20 μM AnCoA4, or left untreated (DMSO treatment) during the infection period. Cells were stained for Rhod-2 (E) or the viral VP1 antigen analyzed using an immunofluorescence assay (F). For each condition, the viral antigen (%) was calculated as described in

Materials and Methods. The experiments were conducted in triplicate, and their means ± SDs are presented. ***$p < 0.001$,**$p < 0.01$, *$p < 0.05$.

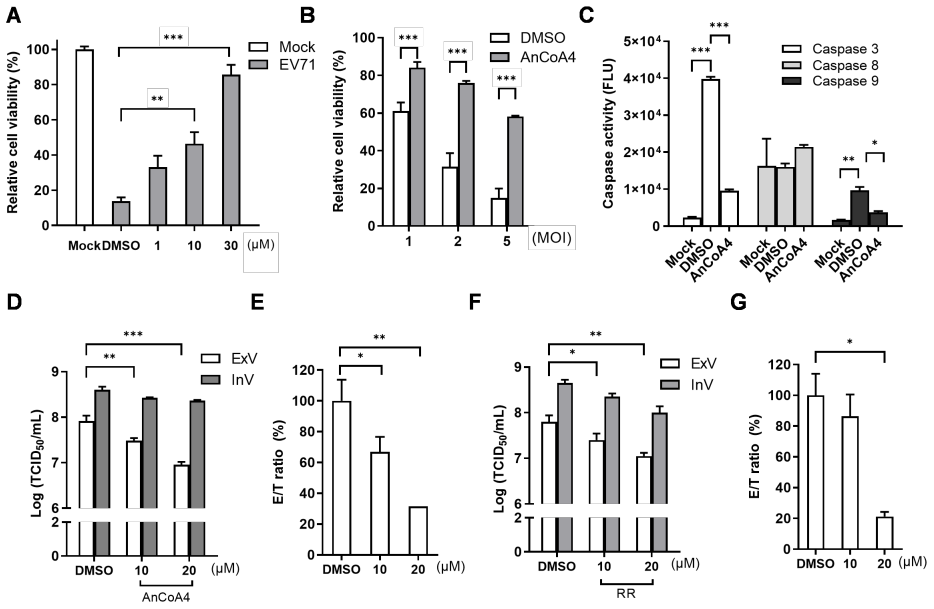

352

FIG 7 The SOCE inhibitor AnCoA4 attenuated EV71-induced apoptosis and the viral release at the late stage of infection. (A) RD cells were mock-infected or infected with EV71 at an MOI of 5 for 12 h. The infected cells were treated with the indicated concentrations of AnCoA4 or left untreated (DMSO). (B) EV71 was used to infect RD cells at MOIs of 1, 2, and 5 for 12 h, and cells were left untreated or treated with 10 μM AnCoA4. Cell viability was measured using the MTS assay and compared with that of mock-infected controls (A, B). (C) RD cells were mock-infected or infected with EV71 at an MOI of 1 for 12 h and treated with 20 μM AnCoA4 during infection or left untreated (DMSO). Caspase-3, -8, and -9 activities were measured using the caspase fluorometric assays. RD cells were infected with EV71 at an MOI of 0.5 for 12 h and treated with AnCoA4 (D) or RR (F), both at 10- and 20-μM, during the infection period. At 12 h p.i., the supernatant was collected for the extracellular virus (ExV), and cells were trypsinized for preparing the intracellular virus (InV). The titers of ExVs and InVs in each group were determined using the $TCID_{50}$ assay (D, F). For each condition, the relative ratio of the ExV titer over the total virus titer, compared with that of untreated control, is represented by the E/T ratio (%) (E, G) and indicates the virus release efficiency. Data represented the means of triplicated experiments and the SD. ***$p < 0.001$,**$p < 0.01$, *$p < 0.05$.

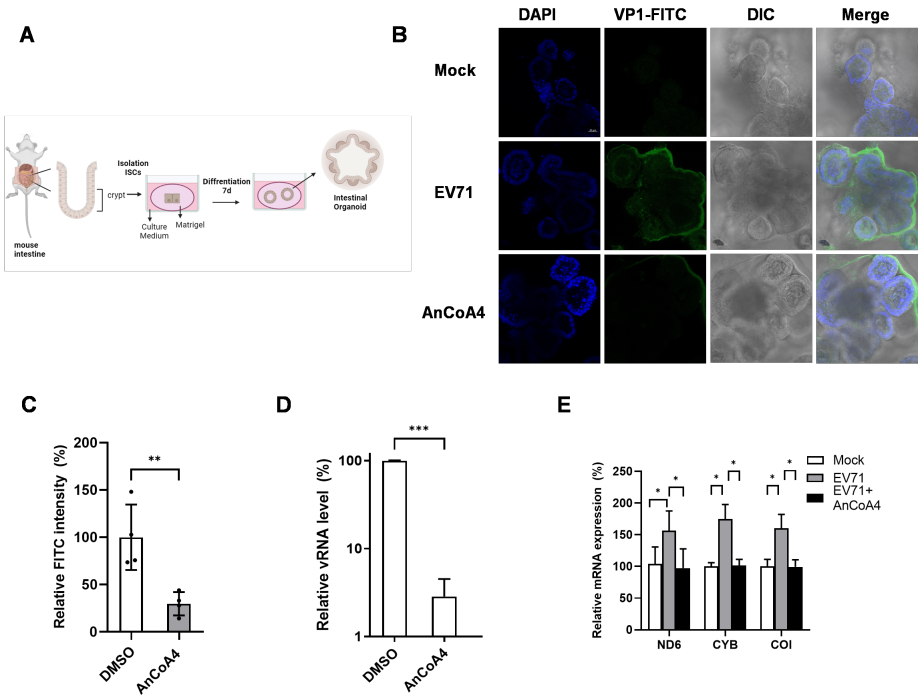

353

FIG 8 EV71 replication and virus-upregulated ETC RNA were reduced by AnCoA4 in the mouse intestinal organoid model. (A) Schematic representation of the three-dimensional mouse intestinal organoid culture. (B) Mouse intestinal organoid cultures seeded in 24-well dishes were inoculated with 200μl EV71 MP4 strain (4×10^8 $TCID_{50}$/mL) for 48 h and treated with 20μM AnCoA4 during the infection period or left untreated (DMSO). Immunofluorescence assay was conducted, with viral VP1 antigen detected using the mouse anti-EV71 Ab (green) and the nucleus stained with DAPI (blue). (C) The green fluorescence intensities of MP4-infected, DMSO-treated, and MP-4 infected, AnCoA4-treated cells were quantified relative to the number of cells stained with DAPI. Total RNA was prepared, and viral RNA (D) and the indicated mitochondrial ETC RNA (E) were measured through RT-qPCR and presented as levels relative to those of the mock-infected controls (%). Data are presented as means ± SDs. ***$p < 0.001$,**$p < 0.01$, *$p < 0.05$.

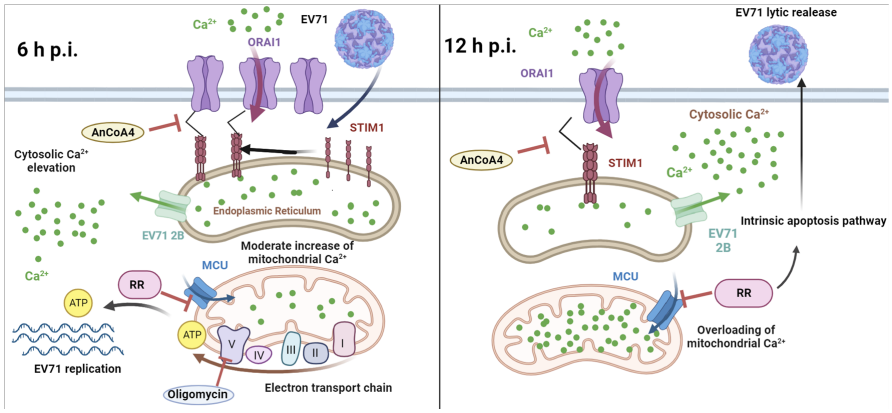

354

FIG 9 Proposed mechanism through which EV71-induced cytosolic Ca^{2+} elevation affects the virus life cycle through SOCE activation and mitochondrial Ca^{2+} influx. EV71 2B caused ER Ca^{2+} depletion, resulting in SOCE activation. At 6 h p.i, cytosolic Ca^{2+} levels increased, causing a moderate elevation in mitochondrial Ca^{2+} and subsequent increases in mitochondrial electron transport chain complex (I through IV) activity and ATP generation for viral replication. At 12 h p.i, overloading of mitochondrial Ca^{2+} promoted viral release through apoptotic cell death triggered by the intrinsic apoptosis pathway. AnCoA4 and RR reduced the levels of cytosolic Ca^{2+} and mitochondrial Ca^{2+}, reducing viral replication and virus release, respectively. Oligomycin targets the mitochondrial complex V (ATP synthase), leading to inhibition of viral replication. RR = ruthenium red. MCU = mitochondrial Ca^{2+} uniporter.

Tables

TABLE 1 Enrichment analysis of biological processes using the DAVID in EV71-infected cells treated with AnCOA4 or left-untreated

Biological process	Gene (Entrez gene ID)[a]	p-value[b]
Electron transport coupled proton transport	MT-ND4, MT-ND5, MT-ND6, MT-CYB, MT-COI	3.15×10^{-3}
Mitochondrial electron transport, NADH to ubiquinone	MT-ND4L, MT-ND4, MT-ND5, MT-ND6	6.68×10^{-3}
ATP synthesis coupled electron transport	MT-ND4L, MT-ND4, MT-ND5, MT-ND6, MT-CYB, MT-COI	6.68×10^{-3}
Response to hydrogen peroxide	MT-ND4, MT-ND5, TXNIP	1.48×10^{-1}
Mitochondrial ATP synthesis coupled proton transport	MT-ND4L, MT-ND4, MT-ND5, MT-ND6, MT-CYB, MT-COI	1.41×10^{-2}
Positive regulation of transcription from RNA polymerase II promoter	CEBPB, KLF15, HOXA, NHLH1, NOG, RGCC, ZC3H12A	6.69×10^{-1}

[a] Gene ID obtained from Entrez Gene resource (https://www.ncbi.nlm.nih.gov/gene/) of NCBI

[b] p-values are adjusted by Bonferroni correction method, which multiplies the raw p-values.

DISCUSSION

In the present study, we integrated confocal microscopy analysis, pharmacological inhibition, RNAi technique, global transcriptome analysis, and live-cell Seahorse assay to define the molecular mechanism underlying the Ca^{2+} flux and its impact on the cell fate and EV life cycle. We showed that the SOCE machinery likely mediated the increase in cytosolic Ca^{2+} and viral replication during the mid-phase of EV71 life cycle (Fig. 1–3). Moreover, we demonstrated that the ETC complex genes were enriched through SOCE during the mid-stage of infection (Table 1). This resulted in alterations in the mitochondrial ETC CI activity, ATP production and cellular respiration (Fig. 4, 5) through SOCE and mitochondrial Ca^{2+} influx, and contributed to viral replication (Fig. 4, 6). The SOCE–mitochondrial Ca^{2+} influx axis also plays a role, at least in part, in triggering apoptosis and subsequent viral release due to mitochondrial Ca^{2+} overload during the late stage of virus infection (Fig. 7). This proposed mechanism (Fig. 9) is supported by our

370 finding that the expression of EV71 2B alone resulted in increases in the ETC transcripts
371 and mitochondrial Ca^{2+} levels (Fig 4B, 6B).

372 The STIM1–Orai1 machinery have been reported to mediate the replication of some
373 viruses. The activation of the STIM1 and Orai1 channels promotes virion assembly and
374 budding during Ebola or Marburg virus infection [37]. The replication capacity of certain
375 viruses, such as dengue virus and rotavirus [38, 39], relies on Ca^{2+} influx through the
376 STIM1–Orai1 system. The hepatitis B virus HBx protein directly binds to and modifies
377 STIM1–ORAI1 complexes, regulating Ca^{2+} levels and thereby promoting viral replication
378 by modulating mitochondrial Ca^{2+} uptake [40]. However, the downstream signaling
379 pathways responsible for their replication remain unknown. Some viruses inactivate
380 SOCE to reduce immune responses and facilitate viral replication. For example, a study
381 reported that the downregulation of type I interferon through Orai1 depletion facilitated
382 SARS-CoV-2 infection [41]. In the current study, we determined that SOCE participates in
383 two steps of the virus life cycle, namely viral replication and virion release, through
384 progressive mitochondrial Ca^{2+} influx. This represents a novel mechanism involving
385 SOCE-mediated virus replication.

386 The findings of our RNA-seq/bioinformatic analysis revealed that a panel of
387 components of mitochondrial ETC complexes were enriched. Because the primary
388 function of mitochondria is to generate ATP through oxidative phosphorylation, we
389 investigated the function correlations between these components and determined that
390 EV71 infection increased mitochondrial ETC CI activity, ATP levels, and cellular
391 respiration. These effects were significantly attenuated following the blockade of SOCE or
392 mitochodrial Ca^{2+} influx by AnCoA4 or RR, respectively. These findings are consistent
393 with those of previous studies indicating that a moderate increase in mitochondrial Ca^{2+}
394 promotes the activities of the ETC CI, CIII, and CIV as well as ATP production [32, 33, 42].
395 Regarding the role of increased ATP in EV replication, studies have demonstrated that EV
396 2C plays a crucial role in virus replication by acting as an ATP-dependent RNA helicase
397 for virus RNA replication. Moreover, EV71 infection induces mitochondrial clustering
398 and recruitment, suggesting localized ATP production occurs at the virus replication site.
399 Prior to this study, some viruses, including cytomegalovirus, dengue virus, and vaccinia

virus, have been reported to promote mitochondrial ETC function and subsequent energy output to support virus replication [31, 30, 43]. Although the mechanisms underlying this phenomenon remain largely unknown for dengue virus and vaccinia virus, the cytomegalovirus protein pUL13 has been demonstrated to interact with mitochondrial cristae to enhance ETC function [31]. To the best of our knowledge, this is the first study to report that EV71 infection augments ETC activity and ATP production to support virus replication and that it employs distinct mechanisms involving SOCE activation and mitochondrial Ca^{2+} influx.

Studies on a diverse group of viruses, including EVs, have revealed that viruses induce substantial and persistent increases in mitochondrial Ca^{2+} levels, leading to apoptotic cell death, especially during the late stages of the infection cycle. In addition to being localized in the ER, the EV71 2B protein was demonstrated to localize to mitochondria, thereby directly binding to and activating the proapoptotic protein Bax [44]. This interaction ensures the induction of cell apoptosis, potentially exacerbating the intrinsic apoptosis driven by mitochondrial Ca^{2+} overload, as demonstrated in this study. Other mechanisms, including EV71-induced, caspase-independent activation of the apoptosis-inducing factor, may contribute to apoptosis, maximizing cell death and virus release.

Human intestinal organoid models have been established and used to study EVs, including EV71 [45, 46, 47]. In this study, we used a mouse intestinal organoid culture system developed from an inbred mouse origin (Fig. 8A). This system offers a stable and continuous supply of organoids, whereas a human model does not [22, 26, 34]. We used the mouse-adapted EV71 strain MP4 for infection, and viral antigen was well discernible in the mouse intestinal organoids in a SOCE-dependent manner (Fig. 8B, C). In addition, we observed a concurrent increase in the levels of mouse ETC ND6, CYB and COI transcripts along with EV71 RNA, all in a SOCE-dependent manner (Fig. 8D, E). These findings indicate that our mouse intestinal organoid system provides a valuable and physiologically relevant platform for in-depth study of virus-induced alterations in host Ca^{2+} signaling.

Our study demonstrated that the SOCE- and mitochondrial Ca^{2+} influx-dependent virus replication can be recapitulated with infections involving other representative EV serotypes (Fig. 6E, F). This led us to speculate whether spatial and temporal control of Ca^{2+} signals, as observed in EV infections, is a common manifestation in viral replication. If this speculation is confirmed, host channels that support these Ca^{2+} signals, such as STIM1 and Orai1, may represent novel targets for the development of broadly effective host-directed antiviral therapeutics.

ACKNOWLEDGMENTS

This study was supported in part by the Professor Tsuei-Chu Mong Merit Scholarship (grant 40719001), NYMU-FEMH Joint Research Program (grant 110DN40), and the Ministry of Science and Technology, Taiwan, ROC (111-2320-B-A49-026-).

Supplemental material

1. supplemental material and method
2. supplemental table
3. supplemental figures

REFERENCES

References

[1] **Baggen J, Thibaut HJ, Strating J, van Kuppeveld FJM**. 2018. The life cycle of non-polio enteroviruses and how to target it. *Nat Rev Microbiol* 16 (6):368–381.

[2] **Liu SL, Pan H, Liu P, Amer S, Chan TC, Zhan J, Huo X, Liu Y, Teng Z, Wang L, Zhuang H**. 2015. Comparative epidemiology and virology of fatal and nonfatal cases of hand, foot and mouth disease in mainland China from 2008 to 2014. *Rev Med Virol* 25 (2):115–28.

[3] **Chami M, Oules B, Paterlini-Brechot P**. 2006. Cytobiological consequences of calcium-signaling alterations induced by human viral proteins. *Biochim Biophys Acta* 1763 (11):1344–62.

[4] **Zhou Y, Frey TK, Yang JJ**. 2009. Viral calciomics: interplays between Ca2+ and virus. *Cell Calcium* 46 (1):1–17.

[5] **Aldabe R, Irurzun A, Carrasco L**. 1997. Poliovirus protein 2BC increases cytosolic free calcium concentrations. *J Virol* 71 (8):6214–7.

[6] **Bozym RA, Morosky SA, Kim KS, Cherry S, Coyne CB**. 2010. Release of intracellular calcium stores facilitates coxsackievirus entry into polarized endothelial cells. *PLoS Pathog* 6 (10):e1001135.

[7] **Campanella M, de Jong AS, Lanke KW, Melchers WJ, Willems PH, Pinton P, Rizzuto R, van Kuppeveld FJ**. 2004. The coxsackievirus 2B protein suppresses apoptotic host cell responses by manipulating intracellular Ca2+ homeostasis. *J Biol Chem* 279 (18):18440–50.

[8] **van Kuppeveld FJ, van den Hurk PJ, van der Vliet W, Galama JM, Melchers WJ**. 1997. Chimeric coxsackie B3 virus genomes that express hybrid coxsackievirus-poliovirus 2B proteins: functional dissection of structural domains involved in RNA replication. *J Gen Virol* 78 (Pt 8):1833–40.

[9] **van Kuppeveld FJ, de Jong AS, Melchers WJ, Willems PH**. 2005. Enterovirus protein 2B po(u)res out the calcium: a viral strategy to survive? *Trends Microbiol* 13 (2):41–4.

[10] **Brisac C, Téoulé F, Autret A, Pelletier I, Colbère-Garapin F, Brenner C, Lemaire C, Blondel B**. 2010. Calcium flux between the endoplasmic reticulum and mitochondrion contributes to poliovirus-induced apoptosis. *J Virol* 84 (23):12226–35.

[11] **Ao D, Sun SQ, Guo HC**. 2014. Topology and biological function of enterovirus non-structural protein 2B as a member of the viroporin family. *Vet Res* 45:87.

[12] **Nieva JL, Madan V, Carrasco L**. 2012. Viroporins: structure and biological functions. *Nat Rev Microbiol* 10 (8):563–74.

[13] **Nieto-Torres JL, Verdia-Baguena C, Castano-Rodriguez C, Aguilella VM, Enjuanes L**. 2015. Relevance of Viroporin Ion Channel Activity on Viral Replication and Pathogenesis. *Viruses* 7 (7):3552–73.

[14] **van Kuppeveld FJ, Hoenderop JG, Smeets RL, Willems PH, Dijkman HB, Galama JM, Melchers WJ**. 1997. Coxsackievirus protein 2B modifies endoplasmic reticulum membrane and plasma membrane permeability and facilitates virus release. *EMBO J* 16 (12):3519–32.

[15] **van Kuppeveld FJ, Galama JM, Zoll J, van den Hurk PJ, Melchers WJ**. 1996. Coxsackie B3 virus protein 2B contains cationic amphipathic helix that is required for viral RNA replication. *J Virol* 70 (6):3876–86.

[16] **Soboloff J, Rothberg BS, Madesh M, Gill DL**. 2012. STIM proteins: dynamic calcium signal transducers. *Nat Rev Mol Cell Biol* 13 (9):549–65.

[17] **Hogan PG, Lewis RS, Rao A**. 2010. Molecular basis of calcium signaling in lymphocytes: STIM and ORAI. *Annu Rev Immunol* 28:491–533.

[18] **Takemura H, Hughes AR, Thastrup O, Putney J J W**. 1989. Activation of calcium entry by the tumor promoter thapsigargin in parotid acinar cells. Evidence that an intracellular calcium pool and not an inositol phosphate regulates calcium fluxes at the plasma membrane. *J Biol Chem* 264 (21):12266–71.

[19] **Shaw PJ, Feske S**. 2012. Regulation of lymphocyte function by ORAI and STIM proteins in infection and autoimmunity. *J Physiol* 590 (17):4157–67.

[20] **Lu JR, Lu WW, Lai JZ, Tsai FL, Wu SH, Lin CW, Kung SH**. 2013. Calcium flux and calpain-mediated activation of the apoptosis-inducing factor contribute to enterovirus 71-induced apoptosis. *J Gen Virol* 94 (Pt 7):1477–85.

[21] **Supasorn O, Tongtawe P, Srimanote P, Rattanakomol P, Thanongsaksrikul J**. 2020. A nonstructural 2B protein of enterovirus A71 increases cytosolic Ca(2+) and induces apoptosis in human neuroblastoma SH-SY5Y cells. *J Neurovirol* 26 (2):201–213.

[22] **Chen Y, Lee SH, Tsai YH, Tseng SH**. 2014. Ischemic preconditioning increased the intestinal stem cell activities in the intestinal crypts in mice. *J Surg Res* 187 (1):85–93.

[23] **Tseng KC, Hsu BY, Ling P, Lu WW, Lin CW, Kung SH**. 2022. Antidepressant Sertraline Is a Broad-Spectrum Inhibitor of Enteroviruses Targeting Viral Entry through Neutralization of Endolysosomal Acidification. *Viruses* 14 (1).

[24] **Wang YF, Chou CT, Lei HY, Liu CC, Wang SM, Yan JJ, Su IJ, Wang JR, Yeh TM, Chen SH, Yu CK**. 2004. A mouse-adapted enterovirus 71 strain causes neurological disease in mice after oral infection. *J Virol* 78 (15):7916–24.

[25] **Huang DW, Sherman BT, Tan Q, Kir J, Liu D, Bryant D, Guo Y, Stephens R, Baseler MW, Lane HC, Lempicki RA**. 2007. DAVID Bioinformatics Resources: expanded annotation database and novel algorithms to better extract biology from large gene lists. *Nucleic Acids Res* 35 (Web Server issue):W169–75.

[26] **Chen Y, Li C, Tsai YH, Tseng SH**. 2019. Intestinal Crypt Organoid: Isolation of Intestinal Stem Cells, In Vitro Culture, and Optical Observation. *Methods Mol Biol* 1576:215–228.

[27] **Cui C, Merritt R, Fu L, Pan Z**. 2017. Targeting calcium signaling in cancer therapy. *Acta Pharm Sin B* 7 (1):3–17.

[28] **Sadaghiani AM, Lee SM, Odegaard JI, Leveson-Gower DB, McPherson OM, Novick P, Kim MR, Koehler AN, Negrin R, Dolmetsch RE, Park CY**. 2014. Identification of Orai1 channel inhibitors by using minimal functional domains to screen small molecule microarrays. *Chem Biol* 21 (10):1278–1292.

[29] **Vaeth M, Maus M, Klein-Hessling S, Freinkman E, Yang J, Eckstein M, Cameron S, Turvey SE, Serfling E, Berberich-Siebelt F, Possemato R, Feske S**. 2017. Store-Operated Ca(2+) Entry Controls Clonal Expansion of T Cells through Metabolic Reprogramming. *Immunity* 47 (4):664–679.e6.

[30] **Barbier V, Lang D, Valois S, Rothman AL, Medin CL**. 2017. Dengue virus induces mitochondrial elongation through impairment of Drp1-triggered mitochondrial fission. *Virology* 500:149–160.

[31] **Betsinger CN, Jankowski CSR, Hofstadter WA, Federspiel JD, Otter CJ, Jean Beltran PM, Cristea IM**. 2021. The human cytomegalovirus protein pUL13

536 targets mitochondrial cristae architecture to increase cellular respiration during
537 infection. *Proc Natl Acad Sci U S A* 118 (32).

538 [32] **Glancy B, Willis WT, Chess DJ, Balaban RS**. 2013. Effect of calcium on the oxidative
539 phosphorylation cascade in skeletal muscle mitochondria. *Biochemistry* 52
540 (16):2793–809.

541 [33] **Territo PR, French SA, Dunleavy MC, Evans FJ, Balaban RS**. 2001. Calcium
542 activation of heart mitochondrial oxidative phosphorylation: rapid kinetics of mVO2,
543 NADH, AND light scattering. *J Biol Chem* 276 (4):2586–99.

544 [34] **Chen Y, Tsai YH, Tseng BJ, Tseng SH**. 2019. Influence of Growth Hormone and
545 Glutamine on Intestinal Stem Cells: A Narrative Review. *Nutrients* 11 (8).

546 [35] **Yamayoshi S, Yamashita Y, Li J, Hanagata N, Minowa T, Takemura T, Koike S**. 2009.
547 Scavenger receptor B2 is a cellular receptor for enterovirus 71. *Nature Medicine* 15
548 (7):798–801.

549 [36] **Huang HI, Lin JY, Chen HH, Yeh SB, Kuo RL, Weng KF, Shih SR**. 2014. Enterovirus
550 71 infects brain-derived neural progenitor cells. *Virology* 468-470:592–600.

551 [37] **Han Z, Madara JJ, Herbert A, Prugar LI, Ruthel G, Lu J, Liu Y, Liu W, Liu X, Wrobel**
552 **JE, Reitz AB, Dye JM, Harty RN, Freedman BD**. 2015. Calcium Regulation of
553 Hemorrhagic Fever Virus Budding: Mechanistic Implications for Host-Oriented
554 Therapeutic Intervention. *PLoS Pathog* 11 (10):e1005220.

555 [38] **Hyser JM, Utama B, Crawford SE, Broughman JR, Estes MK**. 2013. Activation of the
556 endoplasmic reticulum calcium sensor STIM1 and store-operated calcium entry by
557 rotavirus requires NSP4 viroporin activity. *J Virol* 87 (24):13579–88.

558 [39] **Dionicio CL, Pena F, Constantino-Jonapa LA, Vazquez C, Yocupicio-Monroy M,**
559 **Rosales R, Zambrano JL, Ruiz MC, Del Angel RM, Ludert JE**. 2018. Dengue virus
560 induced changes in Ca(2+) homeostasis in human hepatic cells that favor the viral
561 replicative cycle. *Virus Res* 245:17–28.

[40] **Yao JH, Liu ZJ, Yi JH, Wang J, Liu YN**. 2018. Hepatitis B Virus X Protein Upregulates Intracellular Calcium Signaling by Binding C-terminal of Orail Protein. *Curr Med Sci* 38 (1):26–34.

[41] **Wu B, Ramaiah A, Garcia J G, Hasiakos S, Arumugaswami V, Srikanth S**. 2022. ORAI1 Limits SARS-CoV-2 Infection by Regulating Tonic Type I IFN Signaling. *J Immunol* 208 (1):74–84.

[42] **Di Benedetto G, Scalzotto E, Mongillo M, Pozzan T**. 2013. Mitochondrial Ca(2)(+) uptake induces cyclic AMP generation in the matrix and modulates organelle ATP levels. *Cell Metab* 17 (6):965–975.

[43] **Chang CW, Li HC, Hsu CF, Chang CY, Lo SY**. 2009. Increased ATP generation in the host cell is required for efficient vaccinia virus production. *J Biomed Sci* 16 (1):80.

[44] **Cong H, Du N, Yang Y, Song L, Zhang W, Tien P**. 2016. Enterovirus 71 2B Induces Cell Apoptosis by Directly Inducing the Conformational Activation of the Proapoptotic Protein Bax. *J Virol* 90 (21):9862–9877.

[45] **Good C, Wells AI, Coyne CB**. 2019. Type III interferon signaling restricts enterovirus 71 infection of goblet cells. *Sci Adv* 5 (3):eaau4255.

[46] **Zhao X, Li C, Liu X, Chiu MC, Wang D, Wei Y, Chu H, Cai JP, Hau-Yee Chan I, Kak-Yuen Wong K, Fuk-Woo Chan J, Kai-Wang To K, Yuen KY, Zhou J**. 2021. Human Intestinal Organoids Recapitulate Enteric Infections of Enterovirus and Coronavirus. *Stem Cell Reports* 16 (3):493–504.

[47] **Drummond CG, Bolock AM, Ma C, Luke CJ, Good M, Coyne CB**. 2017. Enteroviruses infect human enteroids and induce antiviral signaling in a cell lineage-specific manner. *Proc Natl Acad Sci U S A* 114 (7):1672–1677.